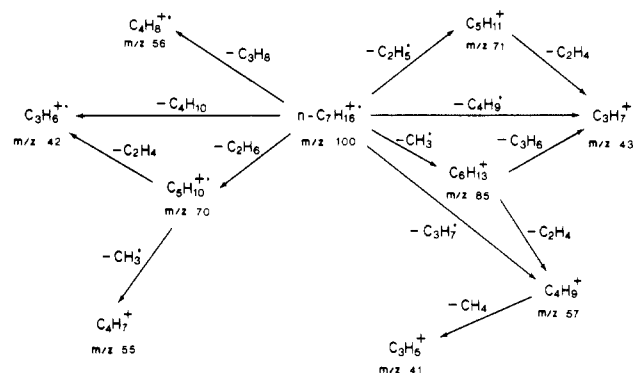


## SCHEME I



with small internal energy can survive to be analyzed as  $m/z$  71.

It has been found that the production of alkyl ions in the photodissociation of *n*-heptane molecular ion occurs directly or consecutively via alkyl ion intermediates. Such alkyl ion fragmentation pathways are well-established by previous investigations.<sup>1,22</sup> Let us compare the present results with the metastable ion decomposition (MID) patterns for the alkyl ions listed in Table II. MID of  $m/z$  85 results in the daughter ions with  $m/z$  57 and 43, in accordance with the present finding. Similarly,  $m/z$  43 is the sole product in the metastable decomposition of  $m/z$  71.

**Alkene and Alkenyl Ions.** It is known that formation of alkene ions from alkane molecular ions proceeds directly or consecutively via alkyl or alkene ion intermediates.<sup>22</sup> Even though some of the propene ions were photoproduced consecutively via pentene ion intermediate (peak E in Figure 4), a rather symmetric shape for the  $m/z$  42 peak indicates that the direct reaction dominated in the production of this ion. On the other hand, it seems that butene and pentene ions were produced directly from *n*-heptane molecular ion, losing propane and ethane, respectively. Since complicated rearrangements of the molecular ion are involved in these reactions,<sup>3</sup> a simple energetical argument would not be adequate to explain the relative intensities of alkene ions in the PD/MIKE spectra.

Two alkenyl ions were produced in the photodissociation of the *n*-heptane molecular ion. Considering that the  $m/z$  55 peak in

Figure 5 generated at the site of photoexcitation tails slowly to peak F, it is likely that most of these ions were produced consecutively via the pentene ion intermediate. If the propenyl ion ( $m/z$  41) were produced directly from the molecular ion, a peak would appear at 2245 eV in the PD/MIKE spectrum of Figure 4. Its absence suggests that the propenyl ion was produced consecutively via the butyl ion only. Metastable decompositions of  $70^{+}$  and  $57^{+}$  gave the same results as photodissociation, as shown in Table II. Namely, all the consecutive dissociation channels observed in the photodissociation could be confirmed indirectly by the metastable ion decomposition patterns, even though the investigated time scales were different. From the results presented so far, the photodissociation channels of *n*-heptane molecular ion can be summarized as in Scheme I.

## V. Summary

Photodissociation of *n*-heptane molecular ion was found to occur through various competing and consecutive reactions. The total photodissociation rate constant was larger than the maximum that could be resolved by the technique employed. Production of propyl ion occurred through three competing dissociation channels, two of which were consecutive reactions while the third seemed to be a direct reaction. The major consecutive reaction was found to occur via a pentyl ion intermediate, and the rate constant for the second step in this reaction was determined. Four other consecutive reaction pathways were identified even though these were not efficient channels in the photodissociation. Based on rough estimations, the fragmentation pathways determined in this work including the consecutive reactions seem to be in agreement with the statistical expectation. More importantly, consecutive dissociation pathways were observed in real time and the rate constant for a consecutive reaction could be determined on a nanosecond time scale. It is expected that the present technique will find wide application in the fundamental study on ion fragmentation kinetics and mechanism.

**Acknowledgment.** This work was supported financially by Yukong Ltd.

**Registry No.**  $C_6H_{13}^+$ , 39749-96-7;  $C_3H_7^+$ , 19252-52-9; *n*-heptane, 34480-77-8.

## Spiral Waves in the Homogeneous and Inhomogeneous Belousov-Zhabotinsky Reaction

R. R. Aliev\* and A. B. Rovinsky\*<sup>†</sup>

*Institute of Theoretical and Experimental Biophysics of the Academy of Sciences, Pushchino, Moscow 142292, USSR (Received: March 26, 1991; In Final Form: August 7, 1991)*

The model of the ferroin-catalyzed Belousov-Zhabotinsky reaction is modified for the temperature range 10–30 °C, which is more appropriate for experiments. In the concentration range explored, a vortex rotates around a stationary circular core. However, in an inhomogeneous medium, it drifts along the boundary of the inhomogeneity. The computations fit experiments well for all measured spiral wave parameters.

## Introduction

Since the pioneering works of Wiener and Rosenblueth,<sup>1</sup> Krinsky,<sup>2</sup> Zhabotinsky and Zaikin,<sup>3</sup> and Winfree,<sup>4</sup> spiral waves in excitable media have been attracting growing attention from researchers from many fields.

Most of the experimental studies on chemical vortex dynamics have been carried out with the ferroin-catalyzed Belousov-Zha-

botinsky reaction. A model of the reaction<sup>5</sup> simulates the behavior of spiral waves qualitatively well. However, the constants of the model fit the experiment at 40 °C while most of the investigations on spirals have been performed at 20–25 °C. Therefore it is hard

- (1) Wiener, N.; Rosenblueth, A. *Arch. Inst. Cardiol. Mex.* **1946**, *16*, 205.
- (2) Krinsky, V. I. *Probl. Kibern.* **1968**, *20*, 59 (in Russian).
- (3) Zhabotinsky, A. M.; Zaikin, A. N. *Oscillatory Processes in Biological and Chemical Systems*; Nauka: Pushchino, USSR, 1971; Vol. 2, (in Russian).
- (4) Winfree, A. T. *Science* **1972**, *175*, 634.
- (5) Rovinsky, A. B. *J. Phys. Chem.* **1986**, *90*, 217.

<sup>†</sup> Present address: Department of Chemistry, University of Toronto, Toronto, ON M5S 1A1, Canada.

to compare the computations and experiments quantitatively. Winfree and Jahnke<sup>6</sup> and Jahnke et al.<sup>7,8</sup> recently compared the results from the calculations and experiments. The calculations were performed with the two-variable Oregonator model. The authors, however, listed several shortcomings of the Oregonator and had to rescale it for better agreement with the experimental data.

This work compares the main characteristics of spiral waves in experiment and in the model Belousov–Zhabotinsky medium with a ferriox ion as catalyst. The rate constants of the model, which were determined for 40 °C, are rescaled for 20 °C in accordance with the Arrhenius law, the activation energy being assumed the same for all the rate constants. Here the computations and the experimental data are compared over wide ranges of the system parameters. Both spatial and temporal periods of spiral waves in the model and real system are in good agreement throughout all the ranges explored.

### The Model Description

The model of the ferriox-catalyzed Belousov–Zhabotinsky (B–Z) reaction in a perfectly stirred vessel has been derived from the Field–Koros–Noyes mechanism:<sup>9,10,5</sup>

$$\frac{\partial x}{\partial \tau} = \frac{1}{\epsilon} \left[ x(1-x) - \left( 2q\alpha \frac{z}{1-z} + \beta \right) \frac{x-\mu}{x+\mu} \right] \quad (1a)$$

$$\frac{\partial z}{\partial \tau} = x - \alpha \frac{z}{1-z} \quad (1b)$$

where

$$\begin{aligned} [\text{Fe}(\text{phen})_3^{2+}] &\equiv Z = Cz, \quad [\text{HBrO}_2] \equiv X = \frac{k_1 A}{2k_4} x, \\ \epsilon &= \frac{k_1 A}{k_4 C}, \quad \alpha = \frac{k_4 K_8 B}{(k_1 A h_0)^2}, \quad \mu = \frac{2k_4 k_7}{k_1 k_5}, \quad t = \frac{k_4 C}{(k_1 A)^2 h_0} \tau, \\ \beta &= \frac{2k_4 k_{13} B}{(k_1 A)^2 h_0}, \quad C = [\text{Fe}(\text{phen})_3^{2+}] + [\text{Fe}(\text{phen})_3^{3+}], \\ A &= [\text{NaBrO}_3], \quad B = [\text{CHBr}(\text{COOH})_2] \end{aligned}$$

$h_0$  is the acidity function,  $q$  is the stoichiometric factor, and  $k_i$  are the rate constants. (There are misprints in the definitions of  $\tau$ ,  $\beta$ , and scaled diffusion coefficients values in refs 5 and 10.)

The function  $h_0$  is used here as the effective proton concentration (unit of measurement is mol/L). The more common acidity function  $H_0$  is considered as a generalization of pH, and these two are related through the equation  $H_0 = -\log(h_0)$ . The use of  $h_0$  instead of the proton concentration proper is reasonable at high concentrations of  $\text{H}_2\text{SO}_4$  (more than 0.1 M).<sup>11–13</sup>

The rate constants were originally estimated for 40 °C.<sup>10</sup> To make it possible to apply the model for different temperatures, we supposed that the rate constants depended on the temperature according to the Arrhenius law with the same activation energy. The activation energy was chosen such that a 20 °C decrease in temperature caused a 10-fold decrease in each rate constant. This “monomolecular” approach was discussed earlier<sup>14–16</sup> and recently

TABLE I: The Rate Constants for the FKN Mechanism

	this paper <sup>a</sup>	“lo” set from ref 18 <sup>a</sup>	data from ref 19 <sup>a</sup>
$k_1$	10	$k_5$	10
$k_4$	$1.7 \times 10^3$	$k_4$	$2 \times 10^3$
$k_5$	$10^6$	$k_2$	$10^6$
$k_7$	1.5	$k_3$	2
$K_8$	$2 \times 10^{-6}$	$b$	$b$
$k_{13}$	$10^{-7}$	$b$	$b$

<sup>a</sup> The unit for  $K_8$  is  $\text{M}^{-1} \text{s}^{-1}$ , for  $k_{13}$  is  $\text{s}^{-1}$ , and for all the others is  $\text{M}^{-2} \text{s}^{-1}$ . <sup>b</sup> No match (specific to the ferriox-catalyzed reaction only).

was implemented for the study of the temperature dependence of the speed of the wave.<sup>17</sup> Thus, the rate constants of model 1 rescaled for 20 °C were

$$k_1 = 10 \text{ M}^{-2} \text{ s}^{-1} \quad k_4 = 1.7 \times 10^3 \text{ M}^{-2} \text{ s}^{-1} \\ k_5 = 10^6 \text{ M}^{-2} \text{ s}^{-1}$$

$$k_7 = 1.5 \text{ M}^{-2} \text{ s}^{-1} \quad K_8 = 2 \times 10^{-6} \text{ M} \text{ s}^{-1} \quad k_{13} = 10^{-7} \text{ s}^{-1} \\ q = 0.5$$

These values are not far from the experimental estimates for several of these constants and are very close to the “Lo” set by Tyson<sup>18</sup> and the data by Field and Foersterling.<sup>19</sup> Although  $K_8$  is a combination of elementary constants ( $K_8 = k_8 k_9 / k_{-8}$ ), it is easily seen that it is rescaled by the same factor as the other constants.

The agreement between the different estimates of the rate constants (Table I) supports the procedure of the temperature rescaling we use here.

Adding to eq 1 diffusion terms yields the reaction–diffusion system

$$\partial x / \partial \tau = F(x, z) + \Delta_\rho x$$

$$\partial z / \partial \tau = G(x, z) + \delta \Delta_\rho z$$

where  $F(x, z)$  and  $G(x, z)$  are the right-hand sides of eqs 1a and 1b, respectively;  $r_i$  are spatial coordinates;  $\rho_i$ 's are the scaled spatial coordinates;  $\Delta_\rho$  is the Laplacian operator with respect to coordinates  $\rho$ ;  $\delta = D_z / D_x$  is the ratio of the diffusion coefficients. The scaling of the  $\rho$  coordinates is given by the expression

$$\rho_i = r_i [(k_1^2 A^2 h_0 / k_4 C) (1 / D_x)]^{1/2}$$

We assume here  $D_x = D_z = 2 \times 10^{-5} \text{ cm}^2 \text{ s}^{-1}$ .

### Spiral Wave Characteristics

Periodic waves of chemical activity spreading from the rotating spiral source, “rotors”, present one of the most interesting ways of self-organization of active media. Creation of the spiral waves both in the experimental and model B–Z chemical mediums is described in the next section. We have studied dependencies of wavelength and rotation period of the waves on the main reactant concentrations as well as on temperature. Figure 1 compares the general views of the spiral wave in the experiment and in the model. Evolution of the rotation period and wavelength with changing concentrations of bromate and acidity of the medium is shown in Figure 2. This figure also presents the period and wavelength calculated with Field–Foersterling constants (Table I). The dependence of the parameters of the wave on temperature is shown by Figure 3. The figure demonstrates that the discrepancy between the experiment and computations becomes significant only below 10 °C.

(6) Winfree, A. T.; Jahnke, W. *J. Phys. Chem.* **1989**, *93*, 2823.  
 (7) Jahnke, W.; Henze, C.; Winfree, A. T. *Nature* **1988**, *336*, 662.  
 (8) Jahnke, W.; Skaggs, W. E.; Winfree, A. T. *J. Phys. Chem.* **1989**, *93*, 740.  
 (9) Field, R. J.; Körös, E.; Noyes, R. M. *J. Am. Chem. Soc.* **1972**, *94*, 8649.  
 (10) Rovinsky, A. B.; Zhabotinsky, A. M.; *J. Phys. Chem.* **1984**, *88*, 6081–6084.  
 (11) Hammett, L. P. *Physical Organic Chemistry*; McGraw-Hill: New York, 1970.  
 (12) *Handbook of Chemistry*; Nauka: Moscow, 1971; Vol. 3.  
 (13) Vavilin, V. A.; Zhabotinsky, A. M.; *Kinet. Katal.* **1969**, *10*, 83–88.  
 (14) Körös, E. *Nature* **1974**, *251*, 703.  
 (15) Blandamer, M. J.; Morris, S. H. *J. Chem. Soc., Faraday Trans. 1* **1975**, *71*, 2319–2330.

(16) Blandamer, M. J.; Morris, S. H. *J. Chem. Soc., Faraday Trans. 1* **1977**, *73*, 1056–65.  
 (17) Kopper, M. T. M.; Schuff, A.; *J. Phys. Chem.* **1990**, *94*, 8135–8139.  
 (18) Tyson, J. J. In *Oscillations and Travelling Waves in Chemical Systems*; Field, R. J., Burger, M., Eds.; 1984.  
 (19) Field, R. J.; Foersterling, H.-D. *J. Phys. Chem.* **1986**, *90*, 5400.

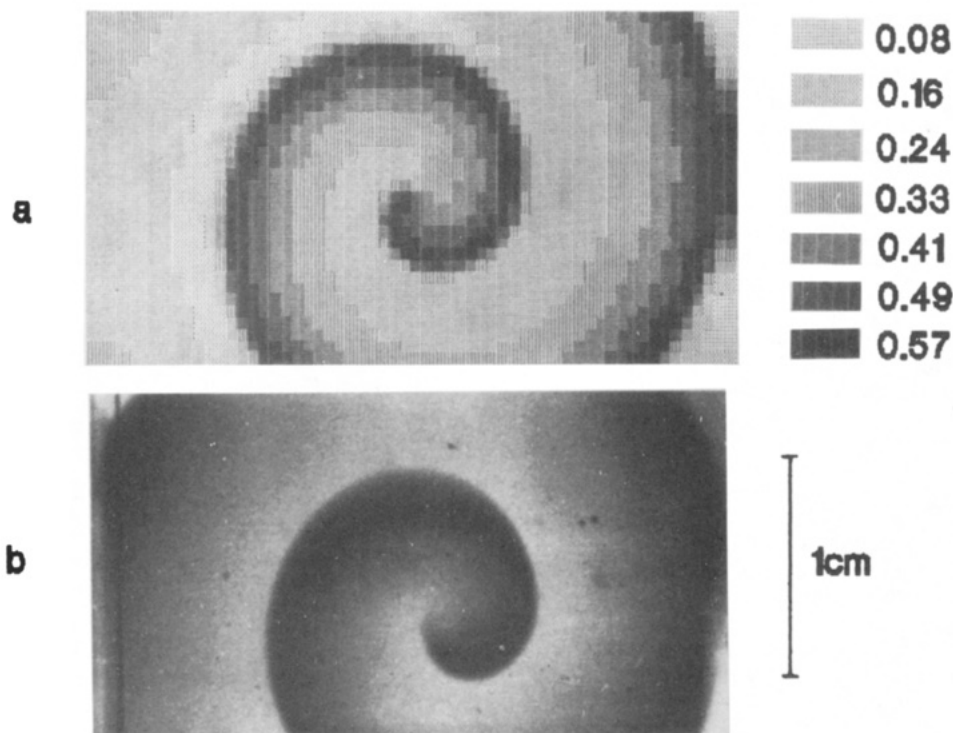


**Figure 1.** (a) Spiral wave in the B-Z reaction by computer simulations. Numbers on the right denote the ferriin concentration in mM/L. (b) Spiral wave in the experimental B-Z reaction. For both cases, the parameters are  $A = 0.05$  M,  $B = 0.05$  M,  $C = 0.65 \times 10^{-3}$  M,  $h_0 = 0.15$  M, and  $t = 20$  °C. The 1-cm scale bar applies to both parts a and b.

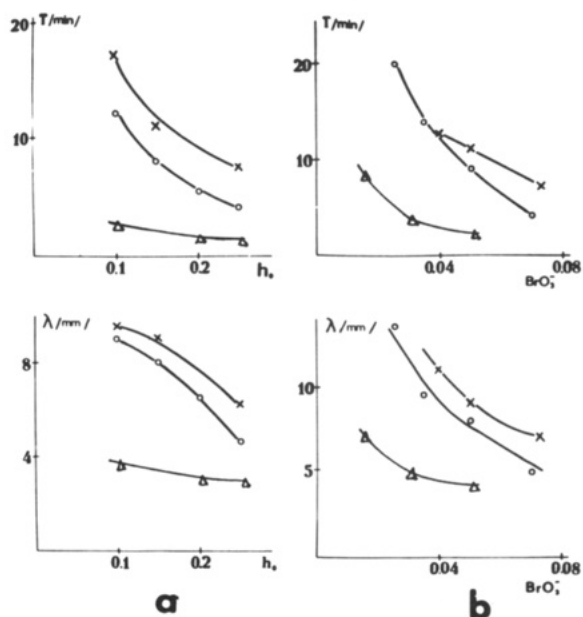


**Figure 2.** Dependence of the rotation period  $T$  (upper row) and wavelength  $\lambda$  (lower row) of the vortex on acidity (a) and bromate concentrations (b). Other parameters are the same as those in Figure 1. Here and in Figures 3–7, crosses denote real experiments in B-Z, while circles denote computer ones. Triangles represent calculations with Field-Foersterlig's constants.<sup>19</sup>

### The Vortex Core

The rotation of the spiral wave can be either stable or unstable. In the case of steady rotation, the tip of the wave traces a circle around the center of rotation within which the medium remains quiet. Otherwise it follows a more or less complex trajectory.<sup>8,26</sup> The quiet area within the circle (if it exists) is called the core of the vortex.<sup>20,21</sup> It is widely believed that the main characteristics of a spiral wave are determined by the behavior of its tip in the

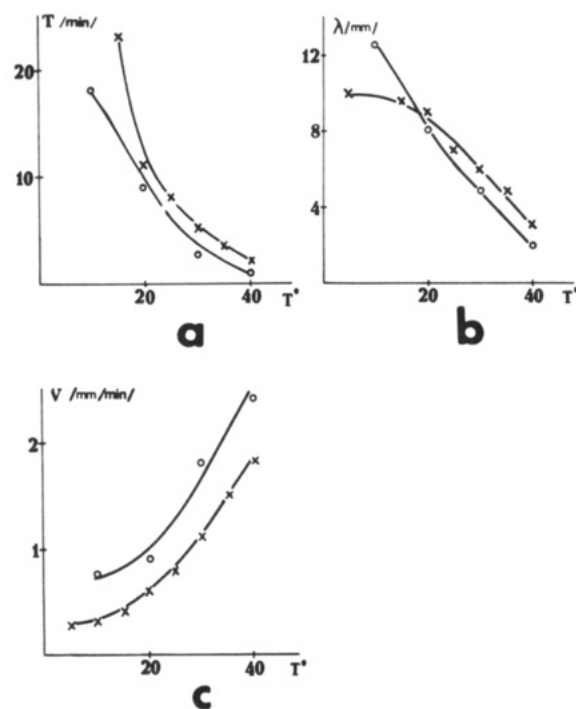


**Figure 3.** Dependence of the rotation period  $T$  (a), wavelength  $\lambda$  (b), and wave velocity  $v$  (c) (which is equal to  $\lambda/T$ ) of a spiral wave on temperature. The B-Z parameters are given in the caption to Figure 1 and  $q = 0.5$ .

vicinity of the core. The steady rotation of a spiral wave around the core was observed both in computer simulations<sup>20</sup> and in the experiments with the Belousov-Zhabotinsky reaction.<sup>21</sup>

In our experiments and computations presented here, spiral waves steadily rotated around a circular core. Figure 4 shows the spatial distribution of the maximal value of ferriin (upper row) and  $\text{HBrO}_2$  (lower row) during the period of rotations of the spiral wave in a computational experiment. One can see that the amplitude of the oscillations near the center of rotation is significantly smaller than those far away from the center at all acidities which

(20) Gulko, F. B.; Petrov, A. A. *Biofizika* **1972**, *17*, 261 (in Russian).  
 (21) Mueller, S. C.; Plesser, T.; Hess, B. *Science* **1985**, *230*, 661.

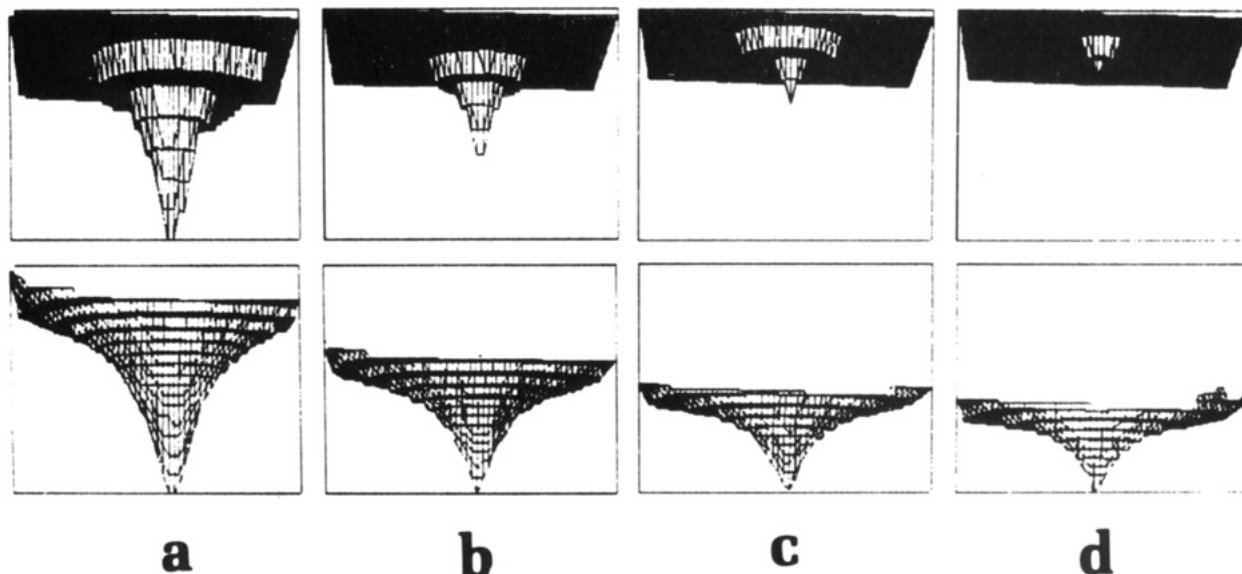


**Figure 4.** Two-dimensional representation of the vortex cores for different proton concentrations: (a)  $h_0 = 0.1$  M; (b)  $h_0 = 0.15$  M; (c)  $h_0 = 0.2$  M; (d)  $h_0 = 0.25$  M. Other parameters are  $A = 0.05$  M,  $B = 0.05$  M,  $C = 0.65 \times 10^{-3}$  M,  $h_0 = 0.15$  M, and  $t = 20$  °C. The upper row is the ferriin concentration distribution; the lower row is the  $[\text{HBrO}_2]$  distribution.

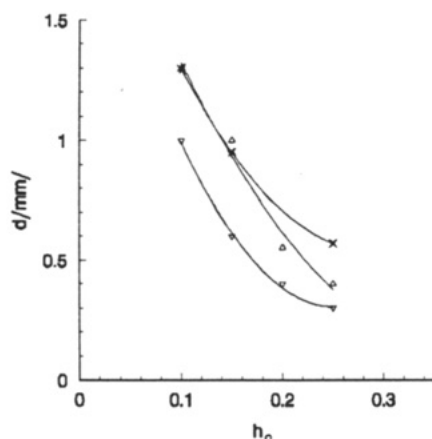


**Figure 5.** The core diameter versus acidity in computations and in the experiment (crosses). Other parameters are the same as those in Figure 1. The level of the ferriin concentration at which the core diameter was measured in the calculations was 0.5 (triangles) and 0.8 (upside down triangles).

have been used (Figure 4a–d). Thus, the core looks like a circled hole around which the wave moves. The experimental section describes how the core size was estimated. The dependence of the diameter on acidity is presented by Figure 5. The size of the core is about 0.1–0.2 of the spiral wavelength and is close to that in the computational results. It should be noted that the diameter of the core was measured in the experiment by analyzing the image created on a photofilm. Unfortunately this procedure does not allow accurate measurements of the ferriin concentration at any particular point of the image. This poses a problem in defining the level of the ferriin concentration at which the core of a spiral should be determined in simulations. For this reason, we calculated the core at two different levels supposing that the experimental level was between the two. In spite of this uncertainty, the agreement between the calculated and measured core sizes is still good for the whole range of the parameter.

#### Drift of the Spiral Wave in an Inhomogeneous Medium

As was stated earlier, we have found in our experiments that spiral waves rotate steadily around a circular core with a fixed center. This steady rotation is likely to be broken in a parametrically inhomogeneous medium. The papers<sup>2,22,23</sup> describe drift

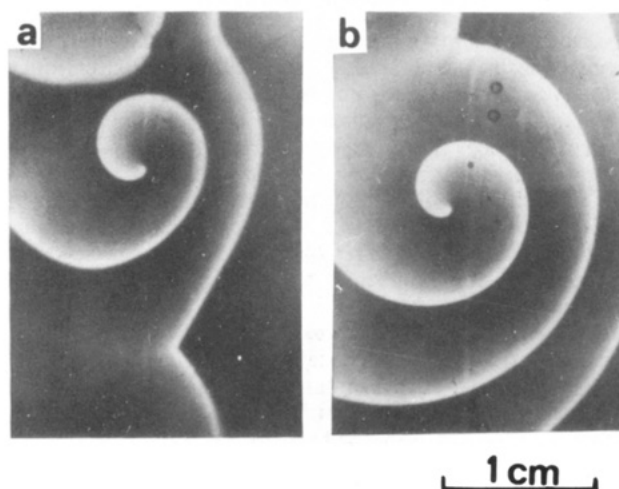


**Figure 6.** Drift of the spiral wave in an inhomogeneous medium: (a)  $t = 25$  min; (b)  $t = 95$  min. At  $t = 0$ , a proton concentration gradient was created; in the right compartment the concentration of sulfuric acid was initially 0.18 M, and in the left one it was 0.12 M.

of spiral waves along a line of inhomogeneity. All papers agree that the direction of the drift should depend on the direction of vortex rotation but come to the opposite conclusions about the particular direction of the drift. Krinsky<sup>2</sup> considers the drift along a homogeneity boundary assuming that the refractory period is longer in the less excitable part of the medium. Pertsov and Ermakova and Davydov et al.<sup>22,23</sup> studied the same problem by supposing the core diameter was smaller in the more excitable part and by neglecting the interaction of a front with the refractory tail of the preceding wave.

We have experimentally studied vortices in the B–Z medium with inhomogeneous acidity distribution. The medium was composed of two contiguous compartments containing sulfuric acid in different concentrations.

Figure 6 shows the displacement of the vortex position with time. The drift gradually slows down because the inhomogeneity diminishes due to proton diffusion. The direction of the drift is determined by the cross product of the angular velocity vector of the vortex and the concentration gradient of the protons. It coincides with that predicted by Krinsky<sup>2</sup> and is opposite to the

(22) Pertsov, A. M.; Ermakova, E. A. *Biofizika* 1988, 33, 338 (in Russian).

(23) Davydov, V. A.; Zykov, V. S.; Mikhailov, A. S.; Brazhnik, P. K. *Izv. Vuzov. Radiofiz.* 1988, 31, 574 (in Russian).

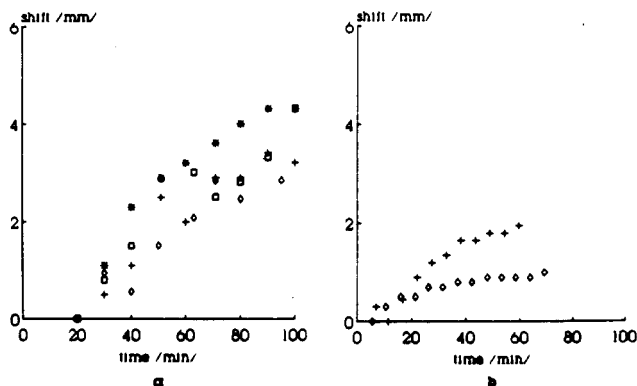


**Figure 7.** Displacement of the vortex with time. The initial moment is the time of the membrane elimination: (a) results of four different runs in the experiment; (b) computational results. Crosses correspond to  $D_h = 2 \times 10^{-5} \text{ cm}^2 \text{ s}^{-1}$  while diamonds to  $D_h = 7 \times 10^{-5} \text{ cm}^2 \text{ s}^{-1}$ .

direction anticipated by Pertsov and Ermakova and Davydov et al.<sup>22,23</sup> This fact supports the conclusion that the refractory tail of excitation plays a significant role in vortex motion.

To simulate the experiments, we have used model 3 with the added equation of proton diffusion:

$$\partial h / \partial t = D_h \Delta h$$

The model medium was also divided into two compartments by an impermeable membrane, and the sulfuric acid concentration in the two parts was made different. Just after the membrane was eliminated, a steep gradient of the acidity as well as a spiral wave was formed. Subsequently the gradient of the proton concentration became smoother due to diffusion. We made computations with two values of the proton diffusion coefficient:  $D_h = 2 \times 10^{-5} \text{ cm}^2 \text{ s}^{-1}$  and  $D_h = 7 \times 10^{-5} \text{ cm}^2 \text{ s}^{-1}$ . The last value was estimated according to ref 24. The results are presented in Figure 7b. Rather surprisingly, the experiment fits the value of  $D_h = 2 \times 10^{-5} \text{ cm}^2 \text{ s}^{-1}$  better. It is interesting that the wavelength  $\lambda$  is greater in the more protonized right compartment than it is in left one. However, the explanation of this fact is obvious: the wave in both parts are synchronized and have the same period  $T$ , but the velocity  $v$  is greater in the more protonized medium and so the wavelength should be greater, since  $\lambda = vT$ .

#### The Experimental and Computational Procedures

**The Experiment.** To avoid intervening hydrodynamic instabilities, we used the B-Z system immobilized in agarose gel.<sup>7,25</sup>

(24) Hodgman, C. D., Ed. *Handbook of Chemistry and Physics*; 1955.

(25) Kuhnert, L. *Naturwissenschaften* 1983, 70, 464.

(26) Plessner, T.; Mueller, S.; Hess, B. *J. Phys. Chem.* 1990, 94, 7501.

To prepare the immobilized system, the melted 1.5% agarose was added to an equal volume of the previously prepared liquid-phase B-Z system (composed of  $\text{NaBrO}_3$ ,  $\text{CH}_2(\text{COOH})_2$ ,  $\text{H}_2\text{SO}_4$ , and ferroin in appropriate concentrations) and carefully mixed. After the medium was cooled to 20 °C and became a solid, it was used for the experiments. The temperature of the experiments was maintained with the precision of 0.2 °C.

A cylindrical wave was initiated with a silver wire of the diameter 0.2 mm. The spiral waves appeared from the front breaks of the cylindrical waves.<sup>2-4</sup> The dynamics of the spirals were recorded by taking snapshots using 35-mm film. The film was further processed for measurements of the wave parameters.

The core of the spiral wave was determined by the following procedure. Snapshots of a vortex were taken at equal time intervals, which were about 0.1 or 0.2 of the rotation period. Then all the images were superimposed. The resulting picture showed that there was an area in the center where the wave did not enter. The circle on which the contrast appeared to be the sharpest (i.e. where the gradient of the ferroin concentration was the largest) was taken as the core. Our technique did not allow us to measure the exact concentration of ferroin on this contour except for the estimate that it was between 0.5 and 0.8 of its maximal value.

The depth of the reaction layer in all the experiments was made large enough (from 3 to 10 mm) to diminish the oxygen effect.

**Calculations.** The computations were performed on a two-dimensional  $50 \times 50$  or  $60 \times 60$  grid. The spatial mesh and temporal step size were chosen such that further increases of the spatial resolution and reductions of the time step could improve the accuracy no more than 10%. The spatial mesh size varied from 0.01 to 0.5 mm but never exceeded 0.025 of the wavelength. The time step was in the range from 0.05 to 0.3 s and was always less than  $10^{-3}$  of the period.

Neumann's (no flux) boundary conditions were imposed on the medium, and Euler's explicit integration method was used. A spiral wave was initiated as follows. First the calculations were carried out in half of the medium ( $25 \times 50$  points). At one of the shorter walls, the concentration of  $\text{HBrO}_2$ , 50 times as great as that of the steady-state value, was fixed for a short time. That end became a planar wave generator. As soon as the wave reached the middle of the reactor, the other half of the medium filled with the species in the steady-state concentrations was added to the first one. Thus a broken wave was created which twisted into a spiral. The wavelength, temporal period, and speed of the wave were measured after 2 or 3 turns of the vortex.

The diameter of the circle within which the amplitude of the Z variable did not exceed 0.5 (or 0.8, in another measurement) of the level far away from the center was regarded as the vortex core.

**Registry No.**  $\text{BrO}_3^-$ , 15541-45-4;  $\text{CH}_2(\text{COOH})_2$ , 141-82-2; ferroin, 14708-99-7.